Remote sensing and geographic information systems methods for global spatiotemporal modeling of biomass burning emissions: Assessment in the African continent

Alicia Palacios-Orueta

Departamento de Silvopascicultura, Escuela Técnica Superior de Ingenieros Montes, Universidad Politécnica de Madrid, Ciudad Universitaria, Madrid, Spain

Alexander Parra and Emilio Chuvieco

Department of Geography, University of Alcalá, Alcalá de Henares, Spain

César Carmona-Moreno

Environment and Sustainability Institute, Global Vegetation Monitoring Joint Research Center, Ispra, Italy

[1] A spatially explicit model for analysis of biomass burning emissions is presented. The model, based on that of *Seiler and Crutzen* [1980], uses satellite images and geographic information systems (GIS) modeling tools to improve the estimation of biomass loads and burning efficiency. The model was assessed in the African continent using the Global Burned Area (GBA-2000) maps derived from SPOT-Vegetation by the Joint Research Center. A total amount of 5711.78 and 336.43 Tg CO was estimated from the model. The areas south of the equator were estimated to release 3579.22 and 218.21Tg CO, while 2132.56 and 118.22 Tg CO were estimated for the Northern Hemisphere. Most of these emissions were generated by two latitude strips: between 3.5° and 11°N, and between 5° and 13°S. Monthly variability shows a clear bimodal temporal behavior, with two maxima in November–February in the northern band and in June–September in the southern band. The effect of biomass loads distribution on gas emissions is clearly shown, with higher gas emissions in the Southern Hemisphere in spite of having lower burned extension.   INDEX TERMS: 3360 Meteorology and Atmospheric Dynamics: Remote sensing; 0315 Atmospheric Composition and Structure: Biosphere/atmosphere interactions; 1615 Global Change: Biogeochemical processes (4805); 1610 Global Change: Atmosphere (0315, 0325); *KEYWORDS:* biomass burning, fire emissions, satellite data

1. Introduction: Issues in Emission Estimations From Biomass Burning

[2] Biomass burning (derived from wildland fires as well as grazing and agricultural fires) is a significant source of carbon to the atmosphere [*Andreae*, 1991]; hence it is an essential factor to consider when evaluating climate changes at a global level. In addition, knowledge of spatiotemporal emission patterns is critical to estimate their effect on atmospheric dynamics and to improve global atmospheric models, as well as to meet international agreements derived from the Kyoto protocol (http://unfccc.int/). Although global fire dynamics are driven by general climatic parameters [*Dwyer et al.*, 2000; *Galanter et al.*, 2000], several authors have pointed out the high interannual and intra-annual variability of biomass burning [*Hoffa et al.*, 1999].

For instance, in tropical areas, temperature and length of the dry season can fluctuate sharply, which strongly affect fire characteristics. Thus, when monitoring emissions at a frequent temporal scale, adjusting parameters according to seasonal variability would be a significant step.

[3] Emission estimations require models adapted at several temporal and spatial scales [*Goldammer*, 1990; *Levine*, 1996; *Prinn*, 1991]. While local estimations and measurements are important to understand emission mechanisms [*Ward et al.*, 1996], regional and global estimations are essential in order to assess emission effects on the atmosphere and on global climate patterns. Models at a high spatial resolution [*Reinhardt et al.*, 1997] provide an evaluation of the spatial variability that global models frequently miss but require more detailed information and are difficult to generalize at global or continental scales. Thus most emission estimation methodologies are adjusted for specific temporal and spatial scales, and their integration is a critical issue to derive consistent and reliable models.

[4] Two main approaches for estimating biomass burning emissions have been proposed in the literature. The first one is based on direct measurements of trace gas released during a fire. This approach has been implemented through field measurements [*Ferek et al.*, 1998; *Goode et al.*, 1999; *Hao et al.*, 1991, 1996], as well through remote sensing analysis of smoke components [*Ferrare et al.*, 1990; *Kaufman et al.*, 1992; *Randriambelo et al.*, 1998]. Both field and remote sensing gas emissions measurements require simultaneity with active fires, either experimental or actual ones. This is difficult owing to operational difficulties to synchronize measurement campaigns with fire activity.

[5] The second approach for emission estimations is based on indirect models that integrate the input variables involved in the process in different manners [*DeFries et al.*, 1999; *DeFries and Townshend*, 1994; *Stroppiana et al.*, 2000]. This approach makes it possible to integrate burnt area maps with independent estimations of input variable values. On the negative side, these studies present more factors of uncertainty caused by error propagation effects when different input variables are considered. Most of these emissions models take into account the biomass loads (i.e., total biomass or available fuel), burning efficiency, burnt areas, and combustion parameters (i.e., combustion efficiency and emission factors or emission ratios) [*Reinhardt et al.*, 1997; *Seiler and Crutzen*, 1980].

[6] Remote sensing is an excellent source of information to derive some of the input parameters required by those models [*Ahern et al.*, 2001; *Barbosa et al.*, 1999; *Stroppiana et al.*, 2000]. Since remote sensors at different resolutions measure the same physical variables (e.g., reflectance and temperature), the use of remotely sensed data in emission models may provide a significant help for spatial scaling, while explicitly considering spatial heterogeneity, mainly when working with input variables at different levels of detail (e.g., fuel types, moisture content, or biomass loads, among others) [*Foody and Curran*, 1994; *Hall et al.*, 1988]. The progress in data fusion techniques may provide a solid framework for this integration in the near future [*Wald*, 1999]. Additionally, the temporal frequency of remote sensing observations may greatly improve time-domain estimations of gas emissions.

2. Objectives

[7] This work presents a strategy to improve the spatio-temporal estimations and analysis of biomass burning emissions at regional and global scales. The model is based on *Seiler and Crutzen*'s [1980]; however, it makes extensive use of satellite images to enhance the spatial assessment of input parameters. Input data processing and statistical analysis of results were based on a geographic information systems (GIS) module (named GFA and integrated in Arc-View™), which was developed for this purpose [*Palacios-Orueta et al.*, 2002]. This article addresses the operability of this system for estimating emissions on a monthly basis and at global scale. The tool contributes to the estimation of global emissions derived from biomass burning and could therefore be used also as a monitoring tool in the implementation of Kyoto protocol.

[8] The assessment of the model was based on estimating CO and CO_2 monthly emissions in the African continent (between 18°N and 35°S) during the year 2000. This study area was selected owing to its importance in global emissions in terms of size and the influence that tropical areas have at global level [*Andreae et al.*, 1996; *Barbosa et al.*, 1999; *Brown and Gaston*, 1996; *Cofer et al.*, 1996; *Delmas et al.*, 1991; *Lacaux et al.*, 1996; *Scholes and Vandermerwe*, 1996; *Ward et al.*, 1996]. However, the GFA module can be easily applied to other study areas, as long as the input data are available.

3. Methods

3.1. Description of the GFA Module

[9] The global fire analysis (GFA) program has two components. The first one (GFA-I) is focused on providing spatial and temporal statistics of burned areas and active fires using thematic layers as classification criterion. It provides both cartographic and table results. The second component (GFA-II) deals with gas emission estimations and is therefore the basis for this paper. The model implemented in GFA-II is based on an indirect approach for gas emissions estimations proposed by *Seiler and Crutzen* [1980], which has been formulated as:

$$M_{i,j,k} = BL_{i,j,m} \times BE_{i,j,m} \times BS_{i,j} \times E_k \times 10^{-15}, \quad (1)$$

where $M_{i,j,k}$ is the amount of gas released for a specific area (with i, j coordinates) in teragrams; $BL_{i,j,m}$ is the biomass load (dry matter) for the same area in grams per square meter (assuming the area has a homogenous cover of fuel/vegetation type m); $BE_{i,j,m}$ is the burning efficiency (i.e., proportion of biomass consumed, $0-1$) of fuel/vegetation type m; $BS_{i,j}$ is burned surface of the same area (m^2); and E_k is the amount of trace gas k released per dry matter unit (g kg^{-1} of biomass).

[10] This equation integrates a set of biophysical variables that can be estimated at several levels of detail, which makes it general enough to be applied at different temporal or spatial scales. The prototype GFA-II code works with the Plate Carré projection since it provides a reasonable balance of cartographic errors when working at global scale. Spatial resolution is 0.00893 squared degrees, which is close to 1 km^2 at the equator; nevertheless, the pixel size can be defined by the user depending on the input data. The results are computed at pixel level, but they are integrated using specific thematic layers defined by the user. Currently, countries, climatic regions, geographical strips, and vegetation units are included in the module.

[11] For the geographical analysis accomplished in this paper, emissions were computed by 0.5° latitude strips, as well as by vegetation types. A more specific analysis was undertaken on the two bands where fire activity is highest (3°−11°N and 5°−13°S). For these areas the temporal evolution of emissions, as well as input variables, will be cross-analyzed.

[12] In the prototype modules a modified version of the Olson map of ecosystem units [*Olson et al.*, 1983] has been selected as the vegetation unit base map because this is still the only map that provides global consistent carbon content values. Olson classes for this work were defined on the basis of their potential to burn, and their carbon contents were revised according to several sources [*Ottmar and*

Table 1. Area and Reference Parameters Used in the GFA-II Model for Each Olson Ecosystem Classes (OCE) in the Study Site[a]

OCE	Area, km^2	BL	OC$_{min}$	OC$_{max}$	BLF	BES	CE	ERCO
Barren deserts volcanos	1,931,732	444	44	444	0.05	0.7	0.95	0.045845
Closed shrubland (scrub)	583,260	10,000	4444	10,000	0.73	0.5	0.91	0.069561
Cropland herbaceous and villages	2,287,324	2196	1556	5556	0.05	0.7	0.96	0.039916
Cropland/grass-woods(field-woods)	1,152,962	3843	6667	6667	0.70	0.4	0.9	0.07549
Evergreen broadleaf forest	2,441,617	21,959	11,111	35,556	0.70	0.2	0.9	0.081419
Forest-field mix (40–60% woods)	209,803	9881	11,111	11,111	0.70	0.45	0.9	0.07549
Grassland	1,825,062	1647	667	1778	0.05	0.96	0.96	0.039916
Open shrubland (semidesert)	2,004,000	2745	1200	2000	0.69	0.5	0.93	0.057703
Permanent wetlands	65,216	3294	4444	15,556	0.20	0.96	0.85	0.105135
Savanna trees (10–30%)	4,206,584	5490	3333	3333	0.70	0.6	0.94	0.051774
Urban/suburban built-up	6110	0	0	3333	0.00	0.1	0	
Woodlands trees (40–60% > 5 m)	1,131,400	19,214	8889	13,333	0.80	0.35	0.916	0.066004
Woody savanna (30–60% > 2 m)	3,396,238	9881	10,000	10,000	0.80	0.45	0.93	0.057703

[a]Here OEC$_{min}$ and OEC$_{max}$ are minimum and maximum biomass loads for each OEC in g m^{-2}; BLF is biomass live fraction; BES is standard burning efficiency; CE is combustion efficiency; and ERCO is emission ratio of CO, as referenced to CO$_2$. Sources are as follows: OEC, J. S. Olson (personal communication, 2002); BLF, R. D. Ottmar (personal communication, 2002, based on the work of *Ottmar and Vihnanek* [1998, 1999, 2000] and *Ottmar et al.*, 2001, 2000a, 1998, 2000b]); BES values, *Akerelodu and Isichei* [1991], *Bilbao and Medina* [1996], *Dignon and Penner* [1996], *Hoffa et al.* [1999], *Hurst et al.* [1994], *Kasischke et al.* [2000], and *Levine* [2000]; CE and ERCO values, *Hao and Ward* [1993], *Delmas et al.* [1995], *Granier et al.* [2000], *Lacaux et al.* [1996], and *Cofer et al.* [1990].

Vihnanek, 1998, 1999, 2000; *Ottmar et al.*, 2001, 2000a, 1998, 2000b; J. S. Olson, personal communication, 2002].

[13] The GFA-II module can work on the basis of either constant average biomass load (BL) and burning efficiency (BE) values for each vegetation type or on spatially distributed values. When using average values, GFA-II assumes no spatial variability within each cover class (hereinafter referred to as Olson ecosystem classes (OEC)). Therefore BL and BE have fixed values for each OEC (both spatially and temporally), taken from literature references (Table 1), and the only source of variation is the map of burned areas input by the user. In the study area, woodlands and savannas show a wide variability in terms of total biomass and fuel availability. For this reason, Olson values have been adjusted for these ecosystems using Ottmar series for quantifying Cerrado fuel in central Brazil. Although the data are not from Africa, they are consistent along a vegetation gradient and therefore more appropriate than using African data from different sources. Thus Cerrado woody and herbaceous vegetation composition has been the main indicator for BE and emission ratios. Burning efficiency values assigned for ''savanna trees,'' ''woodland trees,'' and ''woody savanna'' range from 0.60 to 0.35 on the basis of vegetation size distribution as defined by the Ottmar fuel series from the Brasilian Cerrado, which corresponds approximately to ''Campo sujo,'' ''Cerrado ralo,'' ''Cerrado sensu stricto,'' and ''Cerrado denso,'' where the percentage of woody material ranges from approximately 20 to 90%.

[14] Emission ratios have been approximated according to the amount and size of woody material. A large part of it is composed by medium sizes that are consumed through slow burning and consequently with lower combustion efficiency (CE) and higher CO release.

[15] The second mode for using the GFA-II includes some techniques for addressing the spatial and temporal variability of BL and BE and should provide a more realistic and accurate estimation of these variables. Remote sensing data were selected for this purpose since they provide adequate temporal and spatial variability to monitor vegetation trends. We did not intend to develop new methods for BL and BE estimation from satellite data but rather to take advantage of previous works, adapting them to the global

assessment of both parameters. OEC were used as the starting point of this approach, and satellite time series images were used to refine the spatial and temporal variability included in the OEC original map. The following paragraphs describe how BL and BE were modeled within this spatiotemporal scheme.

3.2. Biomass Loads

[16] The amount of material available to be consumed has been considered as total biomass load (BL). This parameter will be adjusted to the burnable load (i.e., amount of biomass potentially burnt) using the burning efficiency (BE) coefficient of each OEC, as will be explained later.

[17] The estimation of BL in the literature has been approached from field measurements, ecological modeling, and remote sensing methods [*Box et al.*, 1989; *Fazakas et al.*, 1999]. Doubtlessly, it is a complex issue since it involves wide spatial and temporal variability, even within specific species. Consequently, at a global scale, simplifications need to be adopted. For this project the estimation is based on spatial variation of spectral vegetation indices derived from satellite data, which have been extensively used for this purpose [*Box et al.*, 1989; *Ricotta et al.*, 1999; *Sannier et al.*, 2002; *Steininger*, 2000].

[18] For each OEC, biomass load has been bounded according to the maximum and minimum carbon content assigned by J. S. Olson (personal communication, 2002). Biomass load spatial distribution has been estimated from yearly accumulated normalized difference vegetation index (ANDVI) values as a measure of accumulated photosynthetic activity throughout the year.

$$MBL_{i,j} = \left[OC_{min,m} + \left(\frac{ANDVI_{i,j,m} - ANDVI_{min,m}}{ANDVI_{max,m} - ANDVI_{min,m}} \right) \cdot \left(OC_{max,m} - OC_{min,m} \right) \right] / BC, \qquad (2)$$

where $MBL_{i,j}$ is the maximum biomass load (MBL) for pixel i,j; $OC_{min,m}$ and $OC_{max,m}$ are Olson's aboveground carbon minimum and maximum values of MBL for OEC m (in grams of C); $ANDVI_{i,m}$ is the annually accumulated value of NDVI for pixel i,j in OEC m; $ANDVI_{min,m}$ and

$ANDVI_{\max,m}$ are the minimum and maximum accumulated values of NDVI for OEC m; and BC is the factor to convert from grams of C to grams of biomass (in the GFA-II prototype a value of 0.45 was used, which is the most commonly accepted amount of carbon per biomass amount).

[19] The ANDVI was computed as

$$ANDVI_i = \sum_{l=1,12} NDVI_{\max,i,j,l}, \qquad (3)$$

where $NDVI_{\max,i,j,l}$ is the maximum daily NDVI value for month l in each pixel i,j. Selecting the maximum NDVI of a daily time series is a common practice in processing satellite data since daily images may be affected by clouds, atmospheric disturbances, or view-angle effects [Holben, 1986]. As it is well known, NDVI is defined as the normalized ratio of near infrared and red reflectance [Rouse et al., 1974]:

$$NVDI = \frac{\rho_{NIR} - \rho_R}{\rho_{NIR} + \rho_R}, \qquad (4)$$

where ρ_{NIR} and ρ_R refer to the NIR and red reflectance, respectively.

[20] The use of ANDVI as a surrogate of biomass production has been proposed by other authors, who found good correlations between these two variables in several ecosystems [Barbosa et al., 1999; Box et al., 1989]. Obviously, it implies assumptions that are only acceptable when working at a global scale. For instance, NDVI is only sensitive to green biomass, not to those components such as trunks and branches that in many ecosystems represent the largest component of the biomass. Thus this approximation is appropriate for annual herbaceous vegetation, while its adequacy for forest is not so clear. This is because in a full coverage forest, NDVI saturates (during the whole year for an evergreen forest) and also the forest's photosynthetic component represent a low percentage of the total biomass. Therefore this method is more appropriate in areas where forests are not mature and do not have complete coverage (i.e., secondary forests or disturbed forests) where higher NDVI represents higher density. In Africa, most of rain forest fires are located in disturbed areas; therefore this method can be a good approximation for areas with high fire probability. Consequently, although there will be errors in biomass load estimations, these will happen in areas where fire rarely occurs (mature undisturbed forest), and we expect that it will not heavily affect our results.

[21] Monthly maximum NDVI values were computed from a time series of SPOT-Vegetation NDVI 10-day composites (http://www.vgt.vito.be/). The time series cover the period from April 1998 to September 2002 at 1 km^2 pixel size. The images were already available in Plate Carré projection.

3.3. Burning Efficiency

[22] The amount of biomass consumption by the fire is estimated by the burning efficiency (BE) coefficient, defined as the percentage of the total carbon released from the initial stock of carbon contained in the preburn aboveground biomass [Fearnside et al., 2001]. The consumption rate depends on vegetation type and on fire characteristics, especially rate of spread and intensity (which mainly depend on wind, topography, and moisture conditions). Thus BE is composed of a constant structural component that accounts for the amount of material that has a realistic probability of burning (i.e., herbaceous, fine woody material, and litter) and a highly variable component dependent on the environmental conditions that account to a great extent for vegetation moisture. The two extreme classes for Africa in terms of burning efficiency are "broad-leaf evergreen forest" and "grasslands." In the first case the main part of the total biomass is composed of large woody material (trunks and branches), which have a low probability of being burnt, and only the smaller components are usually consumed. In the case of grasslands, most biomass is potentially burnable.

[23] Besides changing along with the vegetation composition, BE also changes seasonally, mainly related to the seasonal trends of moisture content [Fearnside et al., 2001; Hoffa et al., 1999]. As it has been shown by several authors, moisture content of fuels is a critical factor in fire propagation [Viegas, 1998], with less intense and slower fires when fuels are more humid.

[24] Several authors have estimated BE average values for different ecosystem/land cover type from field experiments. These studies rely on measuring biomass consumption in order to characterize the effects of vegetation structure and composition, as well as environmental factors on fire properties [Akerelodu and Isichei, 1991; Bilbao and Medina, 1996; Dignon and Penner, 1996; Fearnside et al., 2001; Hoffa et al., 1999; Hurst et al., 1994; Kasischke et al., 2000; Levine, 2000].

[25] Since fuel moisture estimation has been traditionally based on meteorological danger indices [Viegas et al., 1998], the use of these indices to approximate BE seems a logical approximation [Mack et al., 1996]. However, the global modeling of BE would require meteorological measurements with continuous spatial coverage that is unavailable at a global scale. Thus remote sensing images appear as an alternative way to estimate fuel moisture and, in turn, BE. Some recent studies have addressed the estimation of fuel moisture status from remotely sensed data, both from theoretical and empirical point of views [Ceccato et al., 2001; Chuvieco et al., 2003, 2004; Zarco-Tejada et al., 2003]. They confirm good correlation between NDVI and related indices (such as greenness) with moisture content for grasslands but underline problems in extending such relationships to other vegetation types since NDVI does not include spectral bands in the short wave infrared, which is the most sensitive to water content. However, NDVI has been used by several authors to estimate BE values at global scales. For instance, Barbosa et al. [1999] used relative monthly variations of NDVI values (greenness) as a direct estimation of BE, assuming that NDVI changes throughout the year measure changes in fuel moisture content, as some authors had proposed [Burgan and Hartford, 1993].

[26] The GFA-II approach to estimate BE accounts for both the structural and the environmental factors: it applies BE average values for different ecosystem classes (standard burning efficiency (BES); see Table 1) on the basis of literature references and modifies those values on the basis

of the monthly variation of moisture content, as estimated from the relative greenness. Consequently, the model proposed becomes:

$$\text{BE}_{i,j,l}\left\{\left[1 - \left(\frac{\text{NDVI}_{i,j,l} - \text{NDVI}_{i,j,\min}}{\text{NDVI}_{i,j,\max} - \text{NDVI}_{i,j,\min}}\right)\right] \times \text{BLF}_m + \text{DF}_m\right\} \\ \times \text{BES}_m, \qquad (5)$$

where $\text{BE}_{i,j,l}$ is burning efficiency for pixel i,j in month l; BLF_m and DF_m are the proportions of live and dead fuels in the OEC m (Table 1; $\text{DF} = 1 - \text{BLF}$); and BES_m is the standard burning efficiency values for OEC m (Table 1).

[27] The BLF, DF, and BES parameters are the structural components. Our estimation of BE discriminates between BLF and DF because live and dead fuels show a distinct response to moisture content changes [*Burgan and Rothermel*, 1984]. Burning efficiency of live fuels are assumed to vary inversely along with greenness (the lower the greenness, the drier the fuel, and the higher the BE), while the dead fuels are considered totally consumed in case of a fire. BES accounts for the proportion and size of woody material to herbaceous or foliage biomass. Since we are not using fuel load but biomass load, an overestimation of BE may appear in those ecosystems with a low proportion of foliage biomass. For instance, for an evergreen broadleaf forest the estimated proportion of live fuels is 70%. Therefore, in the driest months, the estimated BE will be close to 1, which is not realistic since this OEC is unlikely to be consumed completely. As a consequence, using the BES threshold, the final BE estimated values will be located on the correct range of variation.

3.4. Burnt Surface

[28] African burnt surface maps for the year 2000 were derived from the Global Burned Areas (GBA-2000) project, which has globally mapped all burned areas based on the analysis of SPOT-Vegetation data [*Grégoire et al.*, 2003]. The project provides burned area regional monthly mosaics for the whole world. For this work the monthly binary files (burned/unburned) were downloaded from the Web page of the project (http://www.gvm.jrc.it/fire/gba2000/gba2000_sources.htm). Optimized algorithms by ecosystems were applied to detect burned surfaces.

3.5. Combustion Efficiency and Emission Ratios

[29] A critical variable in terms of climate studies is the trace gas species distribution, which is directly dependent on the fire combustion efficiency (CE). Combustion efficiency expresses the ratio between the flaming and smoldering phases, which depends on vegetation type and actual fire conditions. Most of the references provide values for the two end-members that represent the more distant CE values, which are the savanna and forest ecosystems. CE is higher during the flaming phase, which is dominant in savanna, while in forest the opposite happens. In general terms, combustion efficiency for grasses can be around 0.95 [*Hao et al.*, 1996; *Ward et al.*, 1992], while for large diameter fuels it is 0.70. Therefore a way to estimate CE can be based on the relative proportion of woody and herbaceous components in a given ecosystem [*Mack et al.*, 1996; *Scholes et al.*, 1996].

Table 2. Monthly Values of Burned Areas and Amounts of Gas Emissions (for CO_2 and CO) in the Study Area (35°S–18°N)

Month	Burned Area, km^2	Burned Area, %	CO_2, Tg	CO_2, %	CO, Tg	CO, %
January	370,580.67	15.44	541.83	9.49	30.55	9.08
February	106,731.67	4.45	169.75	2.97	9.44	2.81
March	58,646.60	2.44	102.72	1.80	5.48	1.63
April	39,936.81	1.66	55.18	0.97	2.77	0.82
May	80,070.30	3.34	174.83	3.06	10.43	3.10
June	248,741.14	10.37	912.09	15.97	57.43	17.07
July	303,981.80	12.67	1206.82	21.13	76.93	22.87
August	200,819.35	8.37	635.91	11.13	38.24	11.37
September	193,049.17	8.04	447.61	7.84	24.58	7.31
October	138,792.83	5.78	304.22	5.33	16.72	4.97
November	168,915.73	7.04	274.37	4.80	14.66	4.36
December	489,543.62	20.40	886.43	15.52	49.21	14.63
Grand total	2,399,809.68	100.00	5711.78	100.00	336.43	100.00

[30] Combustion characteristics are taken into account in the form of emission ratios (ER) or emission factors (EF). While EF is the total amount of trace gas released per unit of dry matter, ER is the ratio between a gas species concentration and CO_2 concentration. The choice between emission ratios or factors is based on data availability. Although the use of EF is more accurate, when working at global or regional levels, ER are more easily available. For this reason the formula implemented in GFA-II was

$$\text{AE}_k = \text{ER}_k \times \text{CE} \times \text{AC} \times \text{CCO}, \qquad (6)$$

where ER_k is a nondimensional emission ratio for gas k relative to CO_2 emissions; CE is the combustion efficiency (nondimensional); AC is the amount of carbon in vegetation (nondimensional; default 0.45); and CCO is the amount of CO_2 per kg of carbon as element (g CO_2/kg C = 3667).

[31] The emission ratios implemented in GFA-II are based on experimental results from several sources (Table 1). Most of the experiments have been accomplished on well-defined ecosystems, and consequently, reference values have been adapted to the characteristics of the OCE classes. The main criterion has been the relative amounts of woody and herbaceous vegetation of each OEC.

4. Results and Discussion

[32] Table 2 shows the annual and monthly distribution of burned areas, as well as estimated CO_2 and CO emissions for the whole study region. According to the GBA maps used in this study, a total of 2,399,809 km^2 were burned in Africa during the year 2000. Following the methods presented in this paper, those fires released a total amount of 5711.78 of CO_2 and 336.43 Tg CO. Despite the different techniques and spatial instruments used, the burned area obtained by *Grégoire et al.* [2003] is within the range of values obtained by other authors. Our gas emission estimates are higher but in the range of other studies on the same continent (Tables 3 and 4). The higher estimations may be caused by higher biomass loads and the consideration of both dead and life fuel and the spatiotemporal variability of the BE. Additionally, the larger amount of emissions could be due to biomass production anomalies during the year 2000. *Anyamba et al.* [2002] found that the transition from El Niño to La Niña during 1999–2000 had significant effect

Table 3. Comparison of Different the Estimates of Burned Area for the Southern African Hemisphere

Parameter	Value			
Reference	Barbosa et al. [1999][a] (year 1989)	Scholes et al. [1996][a,b] (year 1989)	Guido et al. [2003][c] (years 1998–2001)	this work[d] (year 2000)
Burned area, $km^2 \times 10^3$	1541	1684	1160	1081

[a]Value computed for the year 1989.

[b]The burned area was computed based on the vegetation types area and on the correspondent fraction of area burned annually.

[c]Average value computed from the time series 1998–2001.

[d]Value computed from burned areas detected in 2000 from GBA-2000 product [Grégoire et al., 2003].

on biomass production in east and southern Africa, owing to a rearrangement of precipitation patterns shown by NDVI anomalies. Dwyer et al. [2000] had already shown that in the areas where moisture deficit is highly negative or positive, fire number and intensity decreases owing to lack of fuel in the first case and excess of moisture in the second.

[33] From the total area identified as burn scars in the GBA project, 1,081,500 km^2 (45%) were burned in the Southern Hemisphere (0°–35°S) and 1,318,309 km^2 (55%) in the Northern Hemisphere (0°–18°N). However, according to our model, the areas south of the equator released more gasses than the Northern Hemisphere. More specifically, the southern African latitudes released 3579.22 Tg CO_2 (62.66%) and 218.21Tg CO (64.86%), while 2132.56 and 118.22 Tg CO were emitted in the Northern Hemisphere. Therefore the Northern Hemisphere gets more burnings but less emission than the Southern Hemisphere. This fact should be related to the land cover distribution in both latitude belts, as it will be commented later on.

[34] Emission spatial patterns clearly show two bands with higher biomass burning and gas emissions activity located between latitudes 3.5° and 11°N (north band (NB)), and between 4.25° and 12.75°S (south band (SB)) (Figures 1 and 2), which concentrate a total amount of 81.69% of CO emissions and 79.58% of CO_2 emissions of the whole continent, plus more than 72% of total burned area. These two belts have been identified by other authors as well. For instance, Dwyer et al. [2000, p. 174] labeled them as zones with "very high level of fire activity, moderate to long fire season duration, and moderate to large fire agglomerations," which are characterized by climate conditions favorable for vegetation growth and drying of fuel. These results are also consistent with the hemispheric behavior of the global fire activity as described by Cahoon et al. [1992] and Carmona-Moreno et al. [2003].

[35] Figure 2 shows the latitudinal gradient for CO_2 and CO total emissions and emission density computed from latitude strips of 0.5 degrees wide. Absolute emissions refer to the total amount of gas emitted for each latitude strip, while relative emissions consider the different area extension of each latitude strip. In both cases a clear contrast between the Southern and Northern Hemispheres is again observed, with higher values in the former. The relative emissions show even clearer this contrast since the northern strips are more massive. For instance, considering absolute values, the peak of the CO_2 emissions in the Southern Hemisphere is 1.18 times larger than in the Northern Hemisphere, while the CO emissions peak is 1.32 larger in the southern than in the northern peak. In relative terms, taking into account the area covered by each strip, the peak of CO_2 emissions of the Southern Hemisphere is 2.76 times

larger than the Northern Hemisphere and 3.09 with respect to CO emissions.

[36] Figure 3 confirms this divergence between the Southern and Northern Hemisphere. In this case the geographical distribution of CO_2 emissions is compared with latitude variation of burned area. As indicated before, the emissions are higher in the Southern Hemisphere, with the critical peak between 4.25 and 12.75°S, while the highest concentration of burned areas is found in the Northern Hemisphere, especially between 5.25 and 12°N. Considering just the two bands of higher fire occurrence, previously named as SB and NB, the contrasts between the Southern and Northern Hemispheres are also clear. The SB emits 2698.72 Tg CO_2 (47.24% of total CO_2 emissions) and 172.68 Tg CO (51.32% of total CO) and includes 26% of total burned area, while the NB emits 1846.52 Tg CO_2 (32.32%) and 102.16 Tg CO (30.36%) but includes 46% of total burned area.

[37] As indicated beforehand, the main reason for this divergence in gas emissions between the two hemispheres can be linked to their dominant vegetation covers with different burning behaviors, mainly with respect to BL. Figure 3 also shows the latitude distribution of burned biomass. The Southern Hemisphere gets higher biomass burned amounts than the Northern Hemisphere. This contrast is particularly evident when compared to the burned area. The main reason of this divergence is related to land cover distribution.

[38] Figure 4 shows the latitude distribution of some OEC input to the model. Burned areas and CO_2 emissions are also included for better comparison. As previously commented, the burned areas are more extended in the Northern Hemisphere, especially in the fringe between 3 and 13°N. The main ecosystem classes at these latitudes are woody savanna and savanna trees, i.e., grasslands with different tree cover proportion (30–60% for the former; l0–30% for the latter), which have biomass loads in the range of 5400–

Table 4. Comparison of Different Estimates of CO_2 and CO Emissions for the African Continent

	Reference			
	Barbosa et al. [1999][a]	Hao et al. [1996][b]	Duncan et al. [2003][c]	This Work[d]
CO_2, Tg	990–3726	4228	–	5711.78
CO, Tg	4–151	–	173	336.43

[a]Average values computed from time series 1985–1991.

[b]Average value.

[c]Average value computed from the time series 1979–2000.

[d]Values computed from burned areas detected in 2000 from GBA-2000 product [Grégoire et al., 2003].
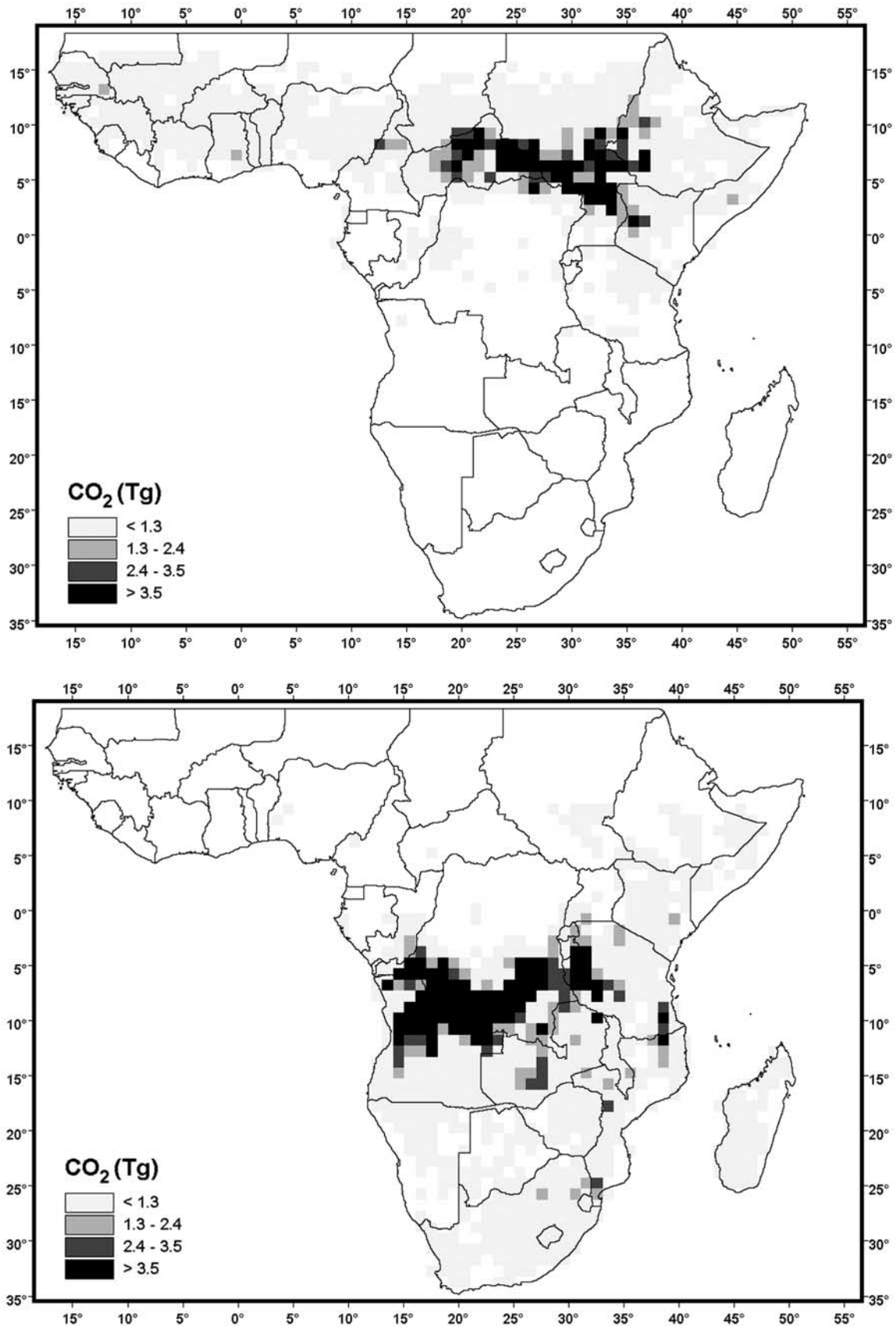
Figure 1. Geographical distribution of CO_2 emissions in the two peak months of fire occurrence for (top) January and (bottom) July. Spatial resolution 1×1 degree.
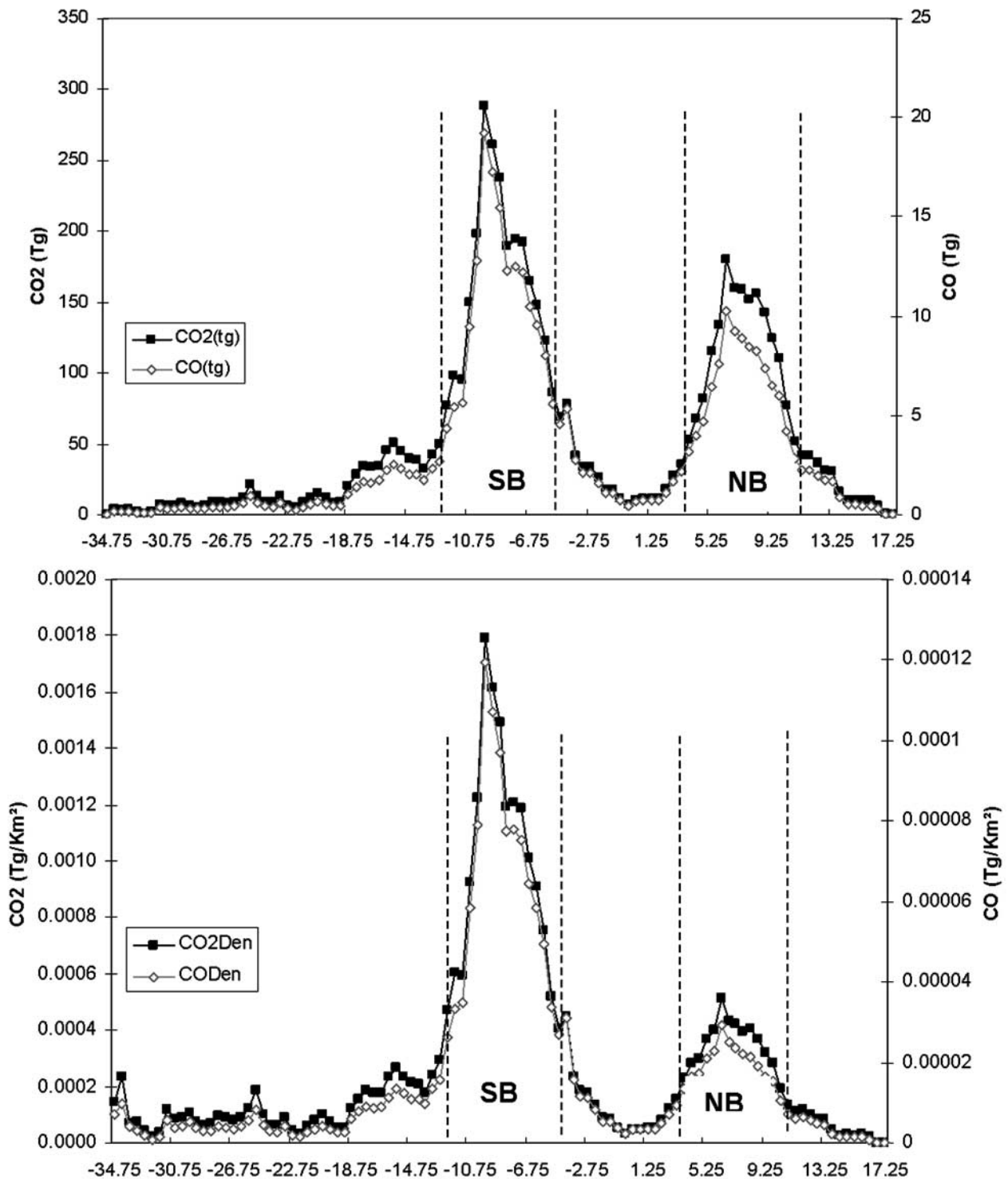
Figure 2. (top) Latitudinal gradient of CO_2 and CO total emissions and (bottom) emission density in the study region.

9800 g m^{-2}. The Southern Hemisphere also has an important proportion of savanna trees but mainly in the band between 12 and 25°S, which is not so severely affected by fire. The highest fire occurrence of this hemisphere is found in the band between 3 and 12°S, which is mainly occupied by woodland trees (more than 30% of the fringe area in most cases) plus evergreen broadleaf and woody

savanna (12–15% each). Woodland trees are grasslands with an important tree cover (40–60% of trees taller than 5 m), while evergreen broadleaf refer to the equatorial primary and secondary forest. Both woodland trees and evergreen broadleaf covers have higher biomass loads than those ecosystems with more extension of savannas, averaging 19,214 and 21,959 g m^{-2}, respectively. It is
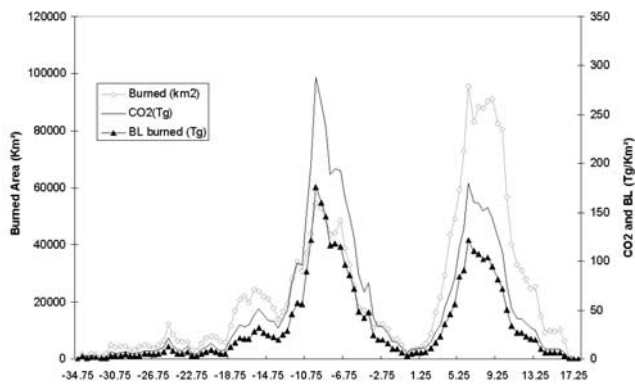
Figure 3. Latitude distribution of CO$_2$ emissions, burned biomass, and burned area.

interesting to note that in those latitude bands where evergreen is predominant (between 4°N and 6°S), fires are much less frequent, corresponding also to the most humid regions of the continent.

[39] The distribution of gas emissions show a clear correlation with burned biomass distribution, as seen in Figure 3, and reflect well the distribution of some OEC covers. While in the Northern Hemisphere, fires burned mainly grass-rich ecosystem units (savanna trees and woody savanna); they have a greater impact on shrubs and tree-covered OECs in the Southern Hemisphere. Consequently, the biomass loads burned are much higher, as is the amount of carbon released to the atmosphere. One can argue that BE values for grass-dominated OEC should be higher than for those more bushy OEC, as is the case in our model, since savanna trees have maximum BE values of 0.65, as opposed to woodland trees with 0.35. Combustion efficiency is higher as well. However, with BL being almost 3 times lower, the multiplication of BL, BE, and CE for savanna trees is still half the value reached by woodland trees and therefore also half the value of the gas emissions produced by this OEC. As stated before, woodland trees are mainly present in the southern band more severely affected by fire and therefore they their presence may explain the divergence between the geographical patterns of burned areas and gas emissions.

[40] Temporal variability of both burned areas and gas emissions shows a bimodal temporal behavior (Table 2) with two maxima in November–February in the NB and in June–September in the SB (Figure 1). OEC classes affected by the fires are also important in terms of potential land use changes and long-term biogenic emission patterns. In savannas the fires occur every year and vegetation recovery is also cyclical, whereas in forest ecosystems a fire may imply a permanent land cover change, increasing biogenic emissions in the long term. This also affects the net CO$_2$ balance since the savannas act as an important CO$_2$ sink every year when savanna regrows rapidly [*Crutzen and Goldammer*, 1993].

[41] The length of the fire period is a significant issue since the dry season duration is not the same either everywhere or every year. Furthermore, it has been shown that fire conditions significantly change along the season [*Hoffa et al.*, 1999]. Thus we tested the consistency between BE temporal changes and burnt areas temporal distribution.

[42] Figure 5 shows the monthly average of BE values together with the monthly BS for the NB and SB where most fires occurred. Temporal trends of burnt areas for each latitude band cross at the end of April and October at a distinct low values. These points may be considered as the onset and the end of the fire season for the each of the Hemispheres. Burning efficiency values for both areas follow similar trends, although less marked. BE lines cross half a month later than BS lines. Since BE may be considered an indicator of dryness, this graph gives an idea of the coupling between the dry season and the burning period. In the south, BE reaches the maximum value in September and keeps decreasing until November–December at the end of the fire season. The fact that BE reaches its maximum value after the fire peak can imply that weather conditions at this time are no longer optimal for fires, but vegetation is still dry and the small number of fires occur at a high BE values. The time evolution of BE is more coupled with BS in the north band: minimum BE happens at the same time that minimum BS, increasing both lines at the same time and reaching the maximum BE and BS in December. This tendency is not so evident in January. The difference in BE patterns between the NB and the SB may be due to the northern savannas faster reaction to dry season in contrast with higher buffer potential of the southern woody ecosystems. Although working at different scale these results reinforces *Hoffa et al.* [1999], who found when working at field level that there was lower fuel consumption in the early dry season. In terms of species distribution, the previous authors found as well that the decrease in combustion efficiency had a larger effect on the release of incomplete combustion products than the percentage of fuel consumed (BE) as well. They found also that to use a single CE value for each ecosystem is not accurate enough because incomplete combustion emissions per unit area were lower during the late dry season.

5. Conclusions

[43] The paper was intended to present a GIS programming tool (named GFA) specifically designed to estimate gas emissions from biomass burning at global scales based on *Seiler and Crutzen* [1980] model. The program makes extensive use of remote sensing input data. These data serve to spatially and temporally interpolate parameters that are critical for indirect estimation of gas emissions, such as biomass loads and burning efficiency. The GFA tool was designed with enough flexibility to include customized parameters for all input variables, as well as to tune up the estimation accuracy in terms of input data layers.

[44] Considering the different assumptions needed when working at global scales, the example presented with African burned areas in 2000 shows that this method provides interesting insights in the spatial and temporal variability of gas emissions and provides new modeling tools for global atmospheric research.

[45] Results show that while biomass burning emissions are highly dependent on burned areas, gas species emission distribution is a function of land cover distribution. Emissions density distribution is particularly sensitive to biomass loads, burning efficiency, and burning conditions. Through remote sensing we can obtain more accurate spatial and
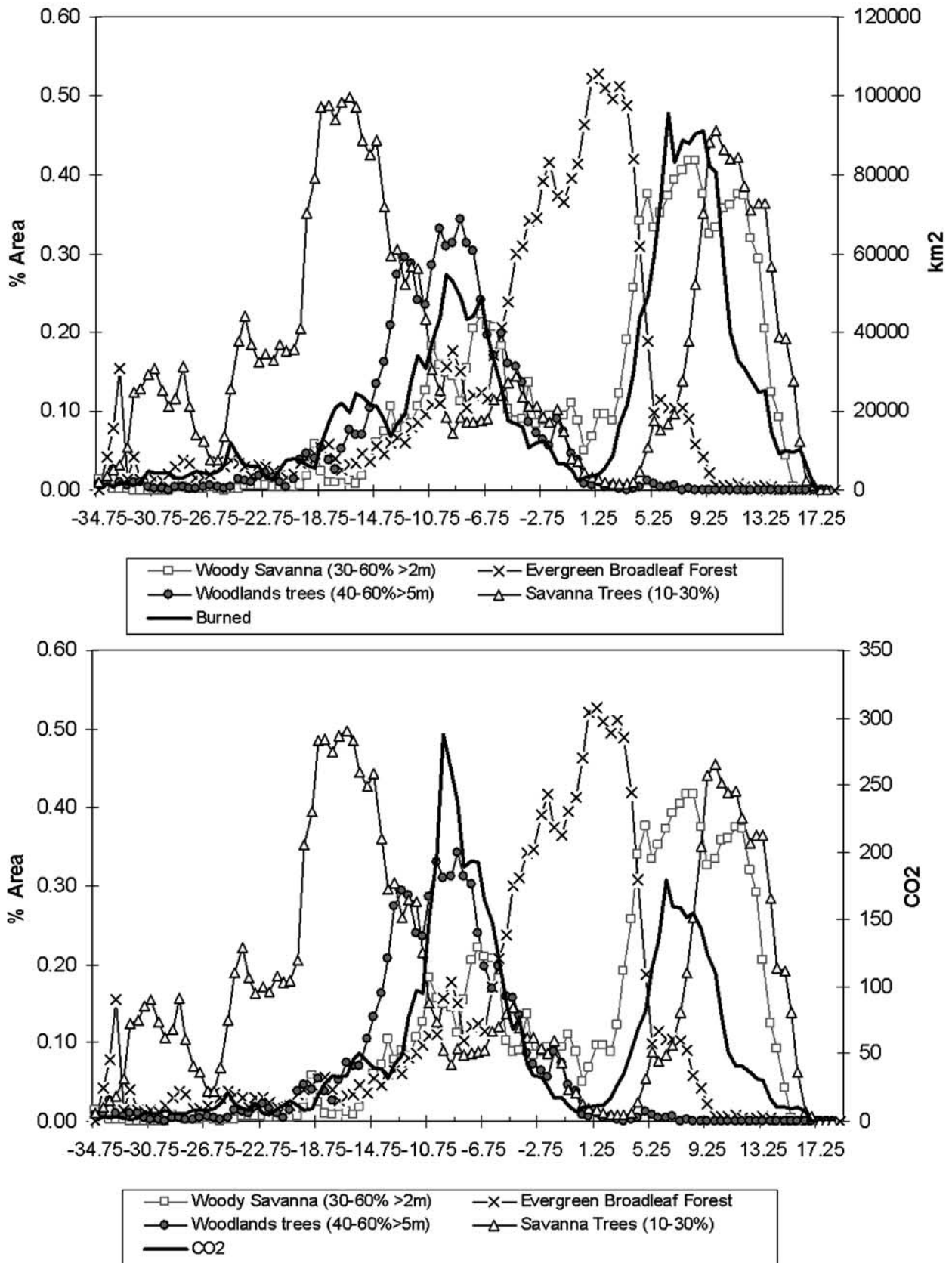
Figure 4. (top) Latitude gradient of burned area and (bottom) CO_2 emissions along with the distribution of some representative OECs.
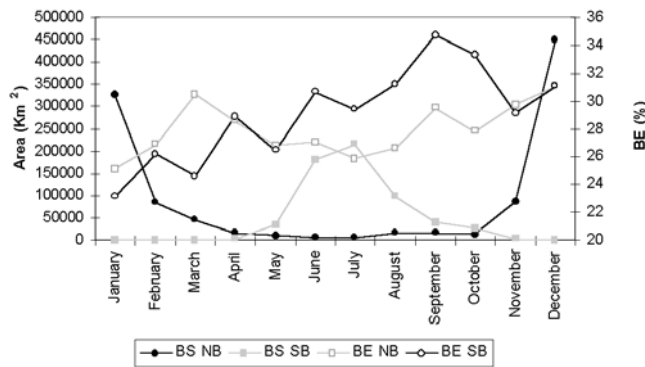
Figure 5. Temporal evolution of burned areas and BE for the two bands most affected by fires.

temporal distribution parameters. Specifically, the combination of BE ecosystem standard values and greenness data allows intraseasonal moisture dynamics to be appropriately included.

References

Ahern, F. J., J. G. Goldammer, and C. O. Justice (2001), *Global and Regional Vegetation Fire Monitoring From Space: Planning a Coordinated International Effort*, SPB Acad. Publ., The Hague.

Akerelodu, F., and A. O. Isichei (1991), Emissions of carbon, nitrogen, and sulfur from biomass burning in Nigeria, in *Global Biomass Burning: Atmospheric, Climatic, and Biospheric Implications*, edited by J. S. Levine, pp. 162–166, MIT Press, Cambridge, Mass.

Andreae, M. (1991), Biomass burning: Its history, use and distribution and its impacts on environmental quality and global climate, in *Global Biomass Burning: Atmospheric, Climatic, and Biospheric Implications*, edited by J. S. Levine, pp. 3–21, MIT Press, Cambridge, Mass.

Andreae, M., J. Fishman, and J. Lindesay (1996), The Southern Tropical Atlantic Region Experiment (STARE): Transport and Atmospheric Chemistry near the Equator–Atlantic (TRACE A) and Southern African Fire-Atmosphere Research Initiative (SAFARI): An introduction, *J. Geophys. Res.*, 101(D19), 23,519–23,520.

Anyamba, A., C. J. Tucker, and R. Mahoney (2002), From El Nino to La Nina: Vegetation response patterns over east and southern Africa during the 1997–2000 period, *J. Clim.*, 15(21), 3096–3103.

Barbosa, P. M., D. Stroppiana, J. M. Gregoire, and J. M. C. Pereira (1999), An assessment of vegetation fire in Africa (1981–1991), Burned areas, burned biomass, and atmospheric emissions, *Global Biogeochem. Cycles*, 13(4), 933–950.

Bilbao, E., and E. Medina (1996), Types of grassland fires and nitrogen volatilization in tropical savannas of Calabozo, Venezuela, in *Biomass Burning and Global Change*, edited by J. S. Levine, pp. 569–574, MIT Press, Cambridge, Mass.

Box, E. O., B. N. Holben, and V. Kalb (1989), Accuracy of the AVHRR vegetation index as a predictor of biomass, primary productivity and net CO_2 flux, *Vegetatio*, 80, 71–89.

Brown, S., and G. Gaston (1996), Estimates of biomass density for tropical forest, in *Biomass Burning and Global Change*, edited by J. S. Levine, pp. 133–139, MIT Press, Cambridge, Mass.

Burgan, R. E., and R. A. Hartford (1993), Monitoring Vegetation greenness with satellite data, U.S. Dep. of Agric. For. Serv., Ogden, Utah.

Burgan, R. E., and R. C. Rothermel (1984), BEHAVE: Fire behavior prediction and fuel modeling system, fuel subsystem, U.S. Dep. of Agric. For. Serv., Ogden, Utah.

Cahoon, D. R., B. J. Stocks, J. S. Levine, W. R. Cofer, and K. P. O'Neill (1992), Seasonal distribution of African savanna fires, *Nature*, 359, 812–815.

Carmona-Moreno, C., J. P. Malingreau, M. Antonovsky, V. Buchshtaber, and V. Pivovarov (2003), Hemispheric fire activity characterization from the analysis of global burned surfaces time series (1982–1993), in *Fourth International Workshop on Remote Sensing and GIS Applications to Forest Fire Management: Innovative Concepts and Methods*, edited by C. Justice, E. Chuvieco, and M. P. Martín, pp. 141–144, Univ. of Ghent, Ghent.

Ceccato, P., S. Flasse, S. Tarantola, S. Jacquemoud, and J. M. Grégoire (2001), Detecting vegetation leaf water content using reflectance in the optical domain, *Remote Sens. Environ.*, 77, 22–33.

Chuvieco, E., I. Aguado, D. Cocero, and D. Riaño (2003), Design of an empirical index to estimate fuel moisture content from NOAA-AVHRR analysis in forest fire danger studies, *Int. J. Remote Sens.*, 24(8), 1621–1637.

Chuvieco, E., D. Cocero, I. Aguado, A. Palacios, and E. Prado (2004), Improving burning efficiency estimates through satellite assessment of fuel moisture content, *J. Geophys. Res.*, 109, D14S07, doi:10.1029/2003JD003467.

Cofer, W. R., J. S. Levine, E. L. Winstead, and B. J. Stocks (1990), Gaseous emissions from Canadian boreal forest fires, *Atmos. Environ. Part A*, 24(7), 1653–1659.

Cofer, W. R., J. S. Levine, E. L. Winstead, D. R. Cahoon, D. I. Sebacher, J. P. Pinto, and B. J. Stocks (1996), Source compositions of trace gases released during African savanna fires, *J. Geophys. Res. Atmos.*, 101(D19), 23,597–23,602.

Crutzen, P. J., and J. G. Goldammer (1993), *Fire in the Environment: The Ecological, Atmospheric, and Climatic Importance of Vegetation Fires: Report of the Dahlem Workshop, Berlin, 15–20 March 1992*, 400 pp., John Wiley, Hoboken, N. J.

DeFries, R. S., and J. R. G. Townshend (1994), Global land-cover: Comparison of ground-based data sets to classifications with AVHRR data, in *Environmental Remote Sensing From Regional to Global Scales*, edited by G. M. Foody and P. J. Curran, pp. 84–110, John Wiley, Hoboken, N. J.

DeFries, R. S., C. B. Field, I. Fung, G. J. Collatz, and L. Bounoua (1999), Combining satellite data and biogeochemical models to estimate global effects of human-induced land cover change on carbon emissions and primary productivity, *Global Biogeochem. Cycles*, 13(3), 803–815.

Delmas, R., P. Loudjani, A. Podaire, and J. C. Menaut (1991), Biomass burning in Africa: An assessment of annually burned biomass, in *Global Biomass Burning: Atmospheric, Climatic, and Biospheric Implications*, edited by J. S. Levine, pp. 126–132, MIT Press, Cambridge, Mass.

Delmas, R., J. P. Lacaux, and D. Brocard (1995), Determination of biomass burning emission factors—Methods and results, *Environ. Monit. Assess.*, 38(2–3), 181–204.

Dignon, J., and J. E. Penner (1996), Biomass burning: A source of nitrogen oxides in the atmosphere, in *Biomass Burning and Global Change*, edited by J. S. Levine, pp. 371–375, MIT Press, Cambridge, Mass.

Duncan, B. N., R. V. Martin, A. C. Staudt, R. Yevich, and J. A. Logan (2003), Interannual and seasonality variability of biomass burning emissions constrained by satellite observations, *J. Geophys. Res.*, 108(D2), 4100, doi:10.1029/2002JD002378.

Dwyer, E., J.-M. Grégoire, and J. M. C. Pereira (2000), Climate and vegetation as driving factors in global fire activity, in *Biomass Burning and Its Inter-Relationships With the Climate System*, edited by J. L. Innes, M. Beniston, and M. M. Verstraete, pp. 171–191, Kluwer Acad., Norwell, Mass.

Fazakas, Z., M. Nilsson, and H. Olsson (1999), Regional forest biomass and wood volume estimation using satellite data and ancillary data, *Agric. For. Meteorol.*, 98–99, 417–425.

Fearnside, P. M., P. M. Lima de Alencastro Graça, and F. J. Alves Rodriguez (2001), Burning of Amazonian rainforests: Burning efficiency and charcoal formation in forest cleared for cattle pasture near Manaus, Brazil, *For. Ecol. Manage.*, 146, 115–128.

Ferek, R. J., J. S. Reid, P. V. Hobbs, D. R. Blake, and C. Liousse (1998), Emission factors of hydrocarbons, halocarbons, trace gases and particles from biomass burning in Brazil, *J. Geophys. Res.*, 103(D24), 32,107–32,118.

Ferrare, R. A., R. S. Fraser, and Y. J. Kaufman (1990), Satellite measurements of large-scale air pollution: Measurements of forest fire smoke, *J. Geophys. Res.*, 95(D7), 9911–9925.

Foody, G., and P. Curran (1994), *Environmental Remote Sensing From Regional to Global Scales*, John Wiley, Hoboken, N. J.

Galanter, M., H. Levy, and G. R. Carmichael (2000), Impacts of biomass burning on tropospheric CO, NO_x, and O_3, *J. Geophys. Res.*, 105(D5), 6633–6653.

Goldammer, J. G. (1990), *Fire in the Tropical Biota: Ecosystem Processes and Global Challenges*, 497 pp., Springer-Verlag, New York.

Goode, J. G., R. J. Yokelson, R. A. Susott, and D. E. Ward (1999), Trace gas emissions from laboratory biomass fires measured by open-path Fourier transform infrared spectroscopy: Fires in grass and surface fuels, *J. Geophys. Res.*, 104(D17), 21,237–21,245.

Granier, C., J.-F. Müller, and G. Brasseur (2000), The impact of biomass burning on the global budget of ozone and ozone precursors, in *Biomass Burning and Its Inter-Relationships With the Climate System*, edited by J. L. Innes, M. Beniston, and M. M. Verstraete, pp. 69–85, Kluwer Acad., Norwell, Mass.

Grégoire, J. M., K. Tansey, and J. M. N. Silva (2003), The GBA2000 initiative: Developing a global burned area database from SPOT-VEGETATION imagery, *Int. J. Remote Sens.*, 24(6), 1369–1376.

Guido, R., J. T. van der Werf, G. J. Randerson, X. Collatz, and L. Giglios (2003), Carbon emissions from fires in tropical and subtropical ecosystems, *Global Change Biol.*, 9(4), 547–562, doi:10.1046/j.1365-2486.2003.00.604.x.

Hall, F. G., D. E. Strebel, and P. J. Sellers (1988), Linking knowledge among spatial and temporal scales: Vegetation, atmosphere, climate and remote sensing, *Landscape Ecol.*, 2(1), 3–22.

Hao, W. M., and D. E. Ward (1993), Methane production from global biomass burning, *J. Geophys. Res.*, 98(D11), 20,657–20,661.

Hao, W. M., D. Scharffe, J. M. Lobert, and P. J. Crutzen (1991), Emissions of N_2O from the burning of biomass in an experimental system, *Geophys. Res. Lett.*, 18(6), 999–1002.

Hao, W. M., D. E. Ward, G. Olbu, and S. P. Baker (1996), Emissions of CO_2, CO, and hydrocarbons from fires in diverse African savanna ecosystems, *J. Geophys. Res.*, 101(D19), 23,577–23,584.

Hoffa, E. A., D. E. Ward, W. M. Hao, R. A. Susott, and R. H. Wakimoto (1999), Seasonality of carbon emissions from biomass burning in a Zambian savanna, *J. Geophys. Res.*, 104(D11), 13,841–13,853.

Holben, B. N. (1986), Characteristics of maximum-value composite images from temporal AVHRR data, *Int. J. Remote Sens.*, 7, 1417–1434.

Hurst, D. F., D. W. T. Griffith, and G. D. Cook (1994), Trace gas emissions from biomass burning in tropical Australian savannas, *J. Geophys. Res.*, 99(D8), 16,441–16,456.

Kasischke, E. S., B. J. Stocks, K. O'Neill, N. H. F. French, and L. L. Bourgeau-Chavez (2000), Direct Effect of fire on the boreal forest carbon budget, in *Biomass Burning and Its Inter-Relationships With the Climate System*, edited by J. L. Innes, M. Beniston, and M. M. Verstraete, pp. 61–71, Kluwer Acad., Norwell, Mass.

Kaufman, Y. J., A. Setzer, D. Ward, D. Tanre, B. N. Holben, P. Menzel, M. C. Pereira, and R. Rasmussen (1992), Biomass burning airborne and spaceborne experiment in the Amazons (Base-A), *J. Geophys. Res.*, 97(D13), 14,581–14,599.

Lacaux, J. P., R. Delmas, C. Jambert, and T. A. J. Kuhlbusch (1996), NO_x emissions from African savanna fires, *J. Geophys. Res.*, 101(D19), 23,585–23,595.

Levine, J. S. (1996), *Biomass Burning and Global Change*, MIT Press, Cambridge, Mass.

Levine, J. S. (2000), Global biomass burning: A case study of the gaseous and particulate emissions released to the atmosphere during the 1997 fires in Kalimantan and Sumatra, Indonesia, in *Biomass Burning and Its Inter-Relationships With the Climate System*, edited by J. L. Innes, M. Beniston, and M. M. Verstraete, pp. 15–31, Kluwer Acad., Norwell, Mass.

Mack, F., J. Hoffstadt, G. Esser, and J. G. Goldammer (1996), Modeling the influence of vegetation fires on the global carbon cycle, in *Biomass Burning and Global Change*, edited by J. S. Levine, pp. 149–159, MIT Press, Cambridge, Mass.

Olson, J. S., J. A. Watts, and L. J. Allison (1983), Carbon in live vegetation of major world ecosystems, Oak Ridge Lab., Oak Ridge, Tenn.

Ottmar, R. D., and R. E. Vihnanek (1998), *Stereo Photo Series for Quantifying Natural Fuels*, vol. II, *Black Spruce and White Spruce Types in Alaska*, U.S. Dep. of Agric. For. Serv., Natl. Interag. Fire Cent., Boise, Idaho.

Ottmar, R. D., and R. E. Vihnanek (1999), *Stereo Photo Series for Quantifying Natural Fuels*, vol. V, *Midwest Red and White Pine, Northern Tallgrass Prairie, and Mixed Oak Types in the Central and Lake States*, U.S. Dep. of Agric. For. Serv., Natl. Interag. Fire Cent., Boise, Idaho.

Ottmar, R. D., and R. E. Vihnanek (2000), *Stereo Photo Series for Quantifying Natural Fuels*, vol. VI, *Longleaf Pine, Pocosin, and Marshgrass Types in the Southeast United States*, U.S. Dep. of Agric. For. Serv., Natl. Interag. Fire Cent., Boise, Idaho.

Ottmar, R. D., R. E. Vihnanek, and C. S. Wright (1998), *Stereo Photo Series for Quantifying Natural Fuels*, vol. I, *Mixed-Conifer With Mortality, Western Juniper, Sagebrush, and Grassland Types in the Interior Pacific Northwest*, U.S. Dep. of Agric. For. Serv., Natl. Interag. Fire Cent., Boise, Idaho.

Ottmar, R. D., R. E. Vihnanek, and J. C. Regelbrugge (2000a), *Stereo Photo Series for Quantifying Natural Fuels*, vol. IV, *Pinyon-Juniper, Sagebrush, and Chaparral Types in the Southwestern United States*, U.S. Dep. of Agric. For. Serv., Natl. Interag. Fire Cent., Boise, Idaho.

Ottmar, R. D., R. E. Vihnanek, and C. S. Wright (2000b), *Stereo Photo Series for Quantifying Natural Fuels*, vol. III, *Lodgepole Pine, Quaking Aspen, and Gambel Oak Types in the Rocky Mountains*, U.S. Dep. of Agric. For. Serv., Natl. Interag. Fire Cent., Boise, Idaho.

Ottmar, R. D., R. E. Vihnanek, H. S. Miranda, M. N. Sato, and S. M. A. Andrade (2001), *Stereo Photo Series for Quantifying Cerrado Fuels in Central Brazil*, vol. I, *Gen. Tech. Rep.*, U.S. Dep. of Agric. For. Serv., Pac. Northwest Res. St., Portland, Oreg.

Palacios-Orueta, A., A. Parra, E. Chuvieco, A. Bastarrika, and C. Carmona (2002), *Global Fire Analysis GIS Modules: Installation and User Manual*, Eur. Commiss., Ispra.

Prinn, R. G. (1991), Biomass burning studies in the International Global Atmospheric Chemistry (IGAC) project, in *Global Biomass Burning: Atmospheric, Climatic, and Biospheric Implications*, edited by J. S. Levine, pp. 22–28, MIT Press, Cambridge, Mass.

Randriambelo, T., S. Baldy, and M. Bessafi (1998), An improved detection and characterization of active fires and smoke plumes in south-eastern Africa and Madagascar, *Int. J. Remote Sens.*, 19(14), 2623–2638.

Reinhardt, E. D., R. E. Keane, and J. K. Brown (1997), *First Order Fire Effects Model FOFEM 4.0: User's Guide, Gen. Tech. Rep. INT-GTR-344*, 65 pp., U.S. Dep. of Agric. For. Serv., Boise, Idaho.

Ricotta, C., G. Avena, and A. D. Palma (1999), Mapping and monitoring net primary productivity with AVHRR NDVI time series: Statistical equivalence of cumulative vegetation indices, *J. Photogramm. Remote Sens.*, 54, 325–331.

Rouse, J. W., R. W. Haas, J. A. Schell, D. H. Deering, and J. C. Harlan (1974), Monitoring the vernal advancement and retrogradation (Green-wave effect) of natural vegetation, NASA Goddard Space Flight Cent., Greenbelt, Md.

Sannier, C. A. D., J. C. Taylor, and W. Duplessis (2002), Real-time monitoring of vegetation biomass with NOAA-AVHRR in Etosha National Park, Namibia, forest fire risk assessment, *Int. J. Remote Sens.*, 23(1), 71–89.

Scholes, R. J., and M. R. Vandermerwe (1996), Greenhouse gas emissions from South Africa, *S. Afr. J. Sci.*, 92(5), 220–222.

Scholes, R. J., D. E. Ward, and C. O. Justice (1996), Emissions of trace gases and aerosol particles due to vegetation burning in Southern Hemisphere Africa, *J. Geophys. Res.*, 101(D19), 23,677–23,682.

Seiler, W., and P. J. Crutzen (1980), Estimates of gross and net fluxes of carbon between the biosphere and the atmosphere from biomass burning, *Clim. Change*, 2, 207–247.

Steininger, M. K. (2000), Satellite estimation of tropical secondary forest above-ground biomass: Data from Brazil and Bolivia, *Int. J. Remote Sens.*, 21(6–7), 1139–1157.

Stroppiana, D., P. A. Brivio, and J.-M. Grégorie (2000), Modelling the impact of vegetation fires, detected from NOAA-AVHRR data, on tropospheric chemistry in tropical Africa, in *Biomass Burning and Its Inter-Relationships With the Climate System*, edited by J. L. Innes, M. Beniston, and M. M. Verstraete, pp. 193–213, Kluwer Acad., Norwell, Mass.

Viegas, D. X. (1998), Fuel moisture evaluation for fire behaviour assessment, in *Advanced Study Course on Wildfire Management, Fin. Rep.*, edited by G. Eftichidis, P. Balabaris, and A. Ghazi, pp. 81–92, Marathon, Coimbra.

Viegas, D. X., J. Piñol, M. T. Viegas, and R. Ogaya (1998), Moisture content of living forest fuels and their relationship with meteorological indices in the Iberian Peninsula, in *III International Conference on Forest Fire Research—14th Conference on Fire and Forest Meteorology*, edited by D. X. Viegas, pp. 1029–1046, Assoc. for Desevolv. Aerodin. Idust., Coimbra.

Wald, L. (1999), Some terms of reference in data fusion, *IEEE Trans. Geosci. Remote Sens.*, 37(3), 1190–1193.

Ward, D. E., R. A. Susott, J. B. Kauffman, R. E. Babbitt, D. L. Cummings, B. Dias, B. N. Holben, Y. J. Kaufman, R. A. Rasmussen, and A. W. Setzer (1992), Smoke and fire characteristics for cerrado and deforestation burns in Brazil: BASE-B experiment, *J. Geophys. Res.*, 97(D13), 14,601–14,619.

Ward, D. E., W. M. Hao, R. A. Susott, R. E. Babbitt, R. W. Shea, J. B. Kauffman, and C. O. Justice (1996), Effect of fuel composition on combustion efficiency and emission factors for African savanna ecosystems, *J. Geophys. Res.*, 101(D19), 23,569–23,576.

Zarco-Tejada, P. J., C. A. Rueda, and S. L. Ustin (2003), Water content estimation in vegetation with MODIS reflectance data and model inversion methods, *Remote Sens. Environ.*, 85, 109–124.

————————

C. Carmona-Moreno, Environment and Sustainability Institute, Global Vegetation Monitoring Joint Research Center, TP 440, Via Fermi 1, I-21020 Ispra (VA), Italy.

E. Chuvieco and A. Parra, Department of Geography, University of Alcalá, Colegios 2, E-28801 Alcalá de Henares, Spain.

A. Palacios-Orueta, Departmento de Silvopascicultura, ETSI Montes, Universidad Politécnica de Madrid, Ciudad Universitaria S/N, E-28040 Madrid, Spain. (apalacios@montes.upm.es)